Article:

Mendez, J.E., Lange, D., Hidalgo, J.P. et al. (1 more author) (2022) Effect of cavity parameters on the fire dynamics of ventilated façades. Fire Safety Journal, 133. 103671. ISSN 0379-7112

https://doi.org/10.1016/j.firesaf.2022.103671

Effect of cavity parameters on the fire dynamics of ventilated façades

*Julian E. Mendez Alvarez [a, *], David Lange [a], Juan P. Hidalgo [a], Martyn S. McLaggan [b]*
[a] *School of Civil Engineering, The University of Queensland, Brisbane St Lucia, QLD, 4072, Australia*
[b] *Department of Civil & Structural Engineering, University of Sheffield, Sheffield S1 3JD, United Kingdom*

**Corresponding author's email: j.mendez@uq.edu.au*

Abstract

Narrow gaps and cavities present in modern construction systems have been identified as one of the key elements that may enable fire spread after an initial fire ignition. Although there are existing models to predict the exposure of the inner linings of a cavity when exposed to a fire, these models have a significant amount of error or are limited to small ranges of application. A parametric experimental study was performed to characterise the fire dynamics in a cavity using a medium-scale non-combustible parallel wall testing rig. Three different cavity widths, three different heat release rates and two air entrainment conditions at the base of the setup (i.e. closed, with no air entrainment at the base; open, with unrestricted air entrainment at the bottom) were varied. Measurements of the flame height and the total external heat flux on the cavity walls were performed. It has been shown that both the heat fluxes and the flame heights increased as the cavity width was reduced. It was found that the radiative component dominates the heat transfer at the bottom of the setup and is less relevant as the height increases, the cavity width increases and the burner output is reduced. Correlations were developed to quantify the heat exposure of a cavity as a function of the geometry of the system, the size of the fire and the ventilation condition. The results obtained can be further used as a baseline in the modelling of upward flame spread in confined spaces featuring combustible linings, and for assessing the potential risks of ignition of combustible elements in ventilated façade systems.

Keywords: fire safety engineering, fire dynamics, ventilated façade, heat flux, flame height.

1. Introduction & Background

Air cavities in façade systems are a common feature of the modern built environment. This void left between two façade elements allows drainage of moisture and acts as a ventilation for the system [1]. However, the presence of an air cavity poses multiple challenges to the fire safety strategy of high-rise buildings. This is because cavities have been identified as a key mechanism of fire spread after an initial fire event, serving as a path for smoke and fire to spread between multiple storeys [2]. This phenomenon was exhibited in previous high rise building incidents, such as the Grenfell Tower fire (2017) where cavity barriers were often either missing or not installed correctly, a fact which may have played a role in enabling the vertical spread of the flame through the cavity between the external cladding and the insulation in the façade system, as well as through small gaps present in the construction environment [3]. Other incidents involving ventilated façades where a cavity could have contributed to the fire spread have been previously reviewed [4].

The current knowledge of the fire behaviour of complex flammable façade systems is extremely limited [5]. Façades in high rise buildings are complex systems which implies the interaction of a number of phenomena that define the fire performance and fire safety outcomes of the façade. It is therefore essential to characterise the fundamental mechanisms that govern the fire response of the system to enable an analysis of the performance of these systems in fire. This requires a characterisation of the effect of varying different attributes of the cavity to provide tools that enable engineers to quantify such performance. This characterisation could be later combined with the available knowledge on the behaviour of different materials comprising the façade system [6].

1.1. Research significance

There is a dearth of knowledge on the vertical flame spread in confined spaces, although it has been identified as a common mechanism for fast fire growth [7]. Fully characterising fire spread through combustible materials in such a configuration requires an understanding of the effect of the system geometry and knowledge on the parameters that govern the underlying fire dynamics in these systems. The study of fire dynamics in facades with non-combustible linings will shed light on how the configuration determines the incident heat flux in the cavity walls. Understanding and being able to predict the heat flux from fire plumes onto the surfaces will then allow a future assessment of the ignition and flame spread on combustible materials in these systems [8]. Determining the distribution of the total external heat flux on the cavity walls is relevant since the energy transferred to the solid governs both the ignition and fire spread over combustible materials. These findings are intended to fit in a bottom-up approach fire safety engineers the tools that allow them to quantify the fire performance of a façade system.

The existing literature on cavity fires has demonstrated the relevance of the distance between the parallel walls as the governing geometrical parameter, as well as the intensity of the fire to explain the dynamics in a cavity fire. Although the differences between existing studies have been commented, there is a need to reconcile the existing results and to find the additional variables that might govern the fire dynamics in cavities.

1.2. Aim and objectives

This paper aims to fully characterise the fire dynamics in a non-combustible parallel wall cavity and explain the differences in behaviour with other non-combustible systems with similar cavities. A medium-scale non-combustible façade system was built to execute a parametric study that sheds light, and allow an investigation of the effect of different variables, on the fire dynamics of the system . The project was developed to quantify the effect of the size of the cavity, the energy source and the air entrainment on the incident heat flux and the flame heights of different enclosed fires. This will provide the necessary baseline for further research to characterise the flame spread over combustible cladding materials at an intermediate scale.

2. Literature review

2.1. Nondimensional groups for a free burning flame

A cavity comprises two surfaces which confine the flame in the event of a fire. To understand the influence of this geometric effect, it is important to first describe the behaviour of an unbounded fire plume. The geometry of turbulent diffusion flames has been found to scale with the square root of the Froude number [9]. The Froude number quantifies the ratio between the momentum forces and the gravitational or buoyancy forces that dictate the shape of a free burning fire (see Eq. 1)

$$\mathrm{Fr} = \frac{u^2}{g \cdot D^2} \tag{1}$$

where u is the gas velocity, g is the acceleration due to gravity and D is the diameter of the flow source. Alternatively, the Froude number can be expressed in terms of the heat release rate (HRR or Q) of the fire and its diameter. The heat release rate can be equated in terms or the burning rate ($\dot{m}$) and the heat of combustion (ΔH_c) as $Q = \dot{m}\Delta H_c$. Further, the burning rate can be expressed as $\dot{m} = \rho u$. Hence, a dimensionless analysis for a circular burner of diameter D leads to the following relationship between Fr, the energy release rate, and the diameter of the source.

$$\mathrm{Fr}\ \alpha\ \frac{Q^2}{D^5} \tag{2}$$

The same analysis for a rectangular burner of width $\mathrm{W_b}$ and length $\mathrm{L_b}$ leads to a relationship of proportionality between the heat release rate per unit length of burner ($\mathrm{Q'}$), the burner width and Fr.

$$\mathrm{Fr}\ \alpha\ \frac{Q^2}{W_b^3 \cdot L_b^2}\ \alpha\ \frac{Q'^2}{W_b^3} \tag{3}$$

The flame geometry can be expressed as the flame height (L_f) normalized by the source width (see Eq. 4).

$$\frac{L_f}{W_b}\ \alpha\ \frac{L_f}{Q'^{\frac{2}{3}}} \tag{4}$$

A further factor that influences the shape and behaviour of the fire plume is the geometry of the burner (i.e. circular vs rectangular, aspect ratio of the rectangular burner). Hasemi and Nishihata determined that there was a significant influence of the fuel shape on flame height and temperature distribution in the plume above the flame, obtaining the shortest flames for a square burner and the longest flames with burners with a large length to width ratio [10]. Other factors influencing the behaviour of the plume include the type of burner used (sand bed vs gas) and the presence of walls that confine the fire.

2.2. Interaction of the fire plume with walls and cavities

The presence of solid surfaces near a flame reduced the area through which air may be entrained across the plume (see Figure 1 a). Previous research has investigated the effect of the presence of one or more walls on the flame height [11]–[13]. Takahashi *et al.* studied the effect of a corner wall on flame height (see Figure 1 a) and found flames were taller compared with free boundary fire [11]. Sugawa *et al.* described the characteristics of flame geometry obtained experimentally from multiple fire sources as a function of the heat release rate and the mixing factor for the flames. The authors observed this factor controls the flame height due to the air entrainment effects. Also, a larger dimensionless flame height was obtained for a burner placed next to a wall compared to a free burning flame coming from a square burner [12]. Hu *et al.* found that flame height decreases with an increase in the separation between the two walls comprising a cavity and that it approaches the value of an unconstrained flame when the cavity width is beyond a critical value, when the shorter side of the burner is perpendicular to the side walls. The authors also found that the air entrainment into the buoyant non-premixed flames for line burners happens mostly from the longer side and rarely from the shorter side of the burner [13].

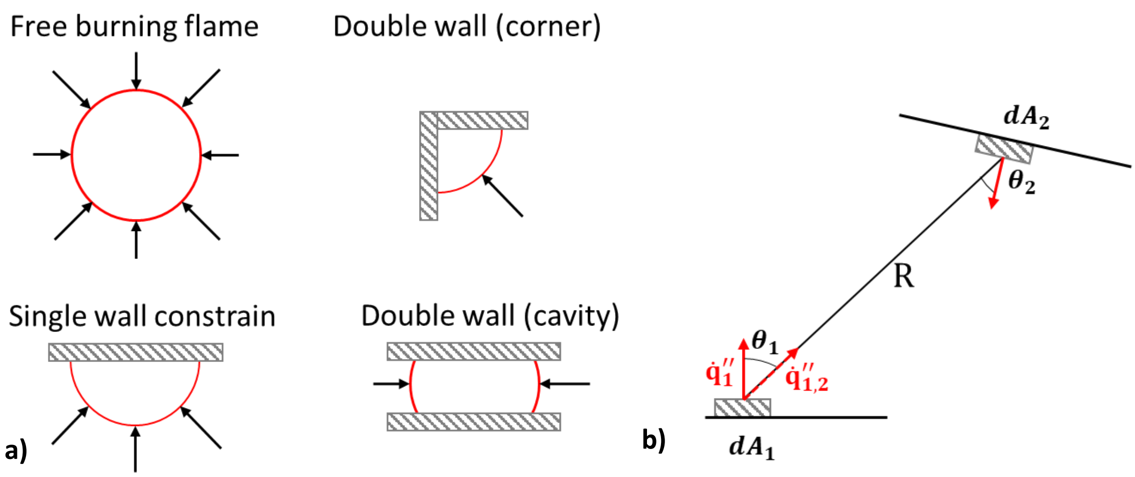

Figure 1. a) Change of air entrainment to the fire plume caused by different configurations b) View factor between two infinitesimal surfaces.

Besides the flame height, the temperature of the plume and the external heat flux on the surfaces changes as the geometry of the system is modified. For example, the presence of a second wall modifies the air flow pattern, affecting the radiative and convective heat transfer compared to a single wall scenario by providing thermal exchange between the two surfaces [14]. The rate of heat transfer between two surfaces, from surface 1 to 2, can be expressed as:

$$\dot{q}_{1,2} = \mathrm{F}_{1,2} A_1 \varepsilon_1 \sigma (T_1^4 - T_2^4) \tag{5}$$

where, $\varepsilon_1$is the emissivity of surface 1, A_1 is the area of surface 1, σ is the Boltzmann constant and T_1 is the temperature of surface 1. The term $\mathrm{F}_{1,2}$ is noted as the integrated configuration factor or view factor and can be expressed as:

$$\mathrm{F}_{1,2} = \frac{1}{A_1} \int_{A_1} \int_{A_2} \frac{cos\theta_1 cos\theta_2}{\pi R^2} dA_1 dA_2 \tag{6}$$

Where R is the shortest distance between the centre points of the surfaces and θ is the angle formed between the vector normal to the surface and the segment R (see Figure 1). This indicates that the view factor (and hence the radiative heat exchange) diminishes as the distance between the surfaces increases. Furthermore, regions located further from the centreline of the surfaces will have smaller view factors.

Additional experimental studies have been performed on the effect on the temperature distribution above the burner [10], [15], and the heat transfer to the surfaces involved [16], [17]. Hasemi and Tokunaga [15] measured the temperature distribution on the fire plumes from square burners in a semi-infinite space (free plume), against a wall and in a corner wall configuration. The decrease of the difference between the plume temperature and the ambient temperature was slower for the case with a wall compared to the free burning flame. Back *et al.* measured the incident heat flux distributions on a wall placed adjacent to a propane burner fire. The heat release rate was found to have a strong impact on the peak heat fluxes [16]. Williamson *et al.* conducted several experiments to determine the effects of heat release rate and the position of the ignition source on the external heat flux distribution on lining materials in corner fire tests. The authors determined that relatively small differences in the ignition source stand-off distance - such as 5 cm - had large effects on the exposure conditions in a room fire. It was determined that a flame impinging the wall led to the most onerous heat flux exposure [17]. If this finding is extrapolated to a cavity scenario, a burner producing a flame that impinges both walls would lead to a more onerous scenario compared to a burner located in the centre of the cavity where the walls are sufficiently far away that there is no flame impingement. This was experimentally shown by Foley, who compared the effect of the ignition source on the heat flux received by parallel walls. The study found that the heat flux to the wall was greater with the burner against that wall, compared to a fire in the centre of the cavity, away from the walls. Foley concluded that moving the burner away from the wall affected the external heat flux by both allowing the convective cooling of the wall and reducing the convective heating from the flame [18], [19]. Further experimental studies have been conducted to characterise the fire dynamics of a cavity, mainly by exploring the influence of the geometry of the system on the flame height and the heat transfer to cavity walls exposed to a flame.

2.3. Previous research on cavity fires

Most research on fire plumes in cavities to date has focused on fires confined to parallel walls [19]–[21] and rack storage systems [22]–[25]. Storage racks were comprised by a main vertical flue and gaps between the racks in the vertical direction, whereas parallel wall systems just feature a main cavity. A diagram of the different setups is presented in Figure 2. All of these systems were comprised of non-combustible materials. The main investigated outputs were the flame height, the gas and solid phase temperatures and the heat flux profile to the surfaces of the cavity between walls or the racks.

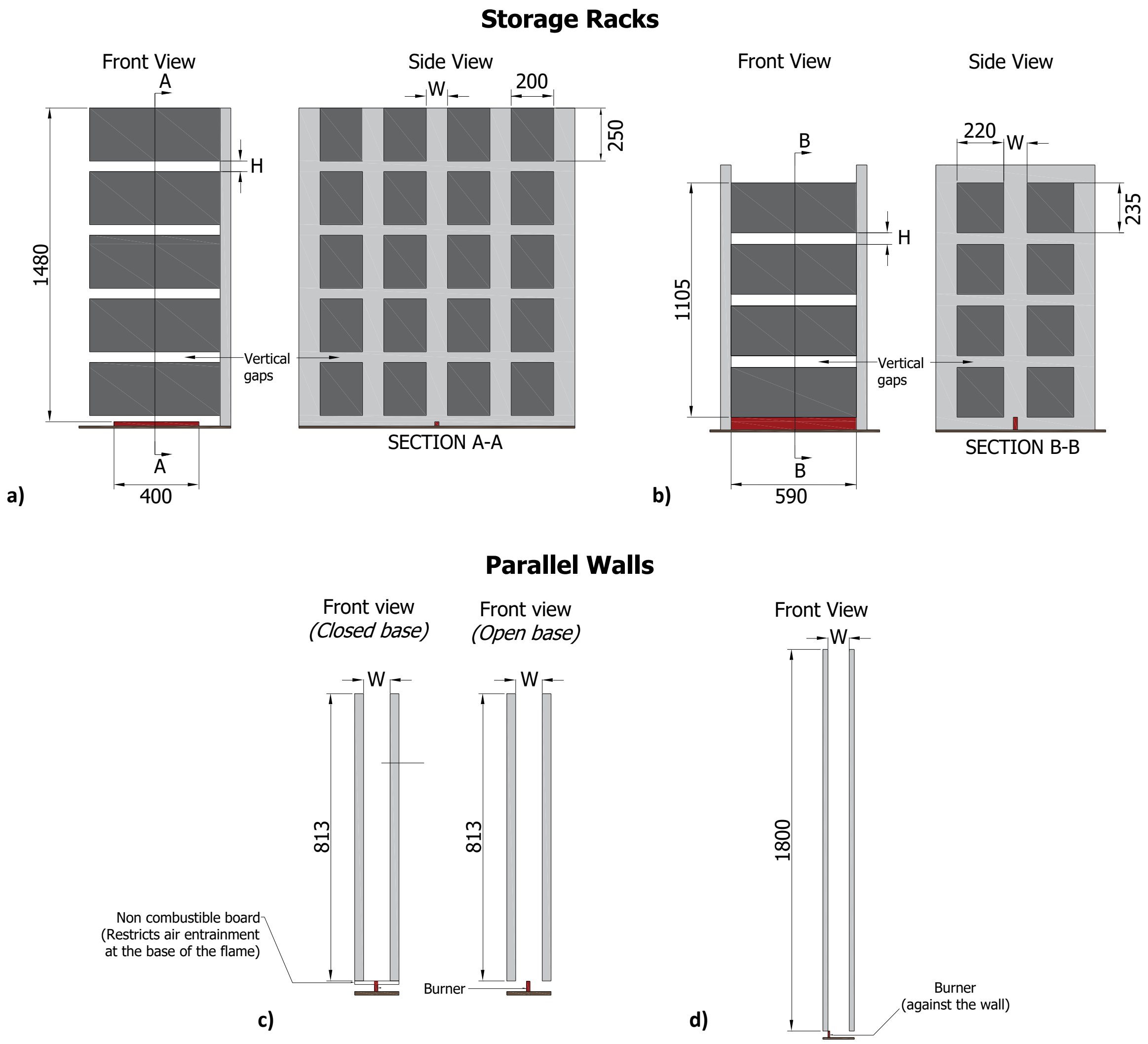

Figure 2. Schematic representation of systems with cavities. a) Storage rack, air entrainment restricted in one direction [22]. b) Storage rack, air entrainment restricted in two directions [23]. c) Parallel walls, different base configurations [19]. **d)** Parallel wall setup, air entrainment restricted in two directions, but not at the base[20].

Karlsson *et al.* developed a correlation between flame height (L_f) and cavity width (W), the spacing between racks (H), and the heat input per unit length of the burner (Q') (see Eq. 7) [22]. The correlation was confined to the setup configurations where W and H had an influence on the flame height. No influence of the geometry and Q' was observed for $W/Q'^{2/3} < 0.007$. The main purpose of this study was to model the behaviour of flames between storage racks (See Figure 2. a). The experimental setup had vertical separations between the racks, in addition to the horizontal separation between the obstructions. Additionally, three sides of the storage rack were open to the environment.

$$\frac{L_f}{Q'^{\frac{2}{3}}} = 0.00242\left(\frac{W}{Q'^{\frac{2}{3}}}\right)^{-0.496} \cdot \left(\frac{H}{Q'^{\frac{2}{3}}}\right)^{-0.07} \quad ; \left(\frac{W}{Q'^{\frac{2}{3}}}\right) < 0.007 \qquad (7)$$

Ingason used a similar experimental setup where two or three sides of the setup were closed in order to restrict the air inflow. A model for the flame height in terms of the heat release rate of the burner and the cavity width was proposed (see Eq.2) [23]. Additionally, Ingason developed a theoretical model for predicting flame heights and temperature profiles in a two-dimensional rack storage system (See Figure 2. b) [25]. Karlsson indicated that the correlations obtained by him and Ingason were significantly different due to the minor differences in the setups (e.g. restriction of air entrainment from 1 of the 4 available sides vs restriction in just 3 of the sides). Ingason stated that the developed models could be applied to other geometries with no lateral openings. The models were limited to the study of the effect of the geometry on the flame height, and no systematic heat transfer measurements were made in this research.

$$L_f = 0.307 + 6.15 \cdot 10^{-4} \cdot \left(\frac{Q'}{W}\right) \tag{8}$$

Foley and Drysdale performed a comprehensive set of tests of fires within a cavity, where the cavity width, the heat release rate of the burner, the burner location (against the wall and at the centre of the cavity), and the air availability (closed and open base) were modified (See Figure 2. c) [19]. The study showed that the availability of air influenced the flame shape as well as the heat flux on the wall. Furthermore, it was demonstrated that the total heat flux to the inner wall increases as the cavity width is reduced. Several empirical correlations were proposed for the incident heat flux as a function of the cavity width (W), the non-dimensional heat release rate per unit length of burner (Q'^*), first introduced by Hasemi [26], and the height across the wall, depending on the configuration of the system. The correlations follow the format of Eq. 9.

$$\dot{q}'' = K_1 \cdot \left(z \cdot \frac{\left(\frac{W}{L_b}\right)^{K_2}}{Q'^{*\frac{2}{3}} \cdot L_b} \right)^{K_3} \tag{9}$$

where $\dot{q}''$ is the total external heat flux on the wall, z is the height above the burner, L_b is the length of the burner, Q'^* is the non-dimensional heat release rate per unit length of burner (see Eq. 10) and K_1, K_2 and K_3 are constants of the model that vary according to the conditions of the system.

$$Q'^* = \frac{Q'}{\rho_\infty \cdot C_p \cdot T_\infty \cdot g^{\frac{1}{2}} \cdot L_b^{\frac{3}{2}}} \tag{10}$$

Livkiss *et al.* [20] obtained a correlation for flame height within a cavity based on experimental data for ventilated façades (See Figure 2. d). The flame heights were measured from 30 photos taken with 1 s intervals after an arbitrary time of 130 s. The authors commented that uncertainties and errors in the measurement could be attributed to factors like the view angle of the camera and the frequency of the flame oscillations relative to the camera shutter speed, among others. The flame height was compared to the studies mentioned before. The discrepancies in the flame height were attributed to the difference in the experimental setups, but these were not quantified. Furthermore, a semi-quantitative analysis of the incident heat flux on the wall as a function of the cavity width and the burner heat release was proposed. It was found that the incident heat fluxes increased as the cavity was made narrower, which matches the conclusion of Foley and Drysdale [19]. Additional research was conducted by de Ris and Orloff on a fire burning between two parallel plates. The authors measured flame heights and flame heat-flux distributions for a wide range of fuels and determined that the heat flux from the flames is sensitive to the flame sootiness. The distance between the panels was kept constant at 300 mm and hence, it was not considered as a variable for a theoretical model for the heat flux distribution along the walls [21].The outcomes of this last study are not included in the following comparison since studying the effect of the cavity width was one of the main objectives of the present research.

A comparison of the experimental setups and the range of the variables used in each of the studies described is presented in Table 1.

Table 1. Experimental conditions for different authors that studied cavity flames.

	Base	*Flame location*	*HRR per unit length of burner* $[\mathbf{kW.m^{-1}}]$	*Cavity width* (W) $[\mathbf{m}]$	*Vertical gaps width* (H)$[\mathbf{m}]$
Foley & Drysdale [19]	Open Closed	Centre of the cavity Near the wall	11.6, 20.9	0.06, 0.1, one wall	N/A
Karlsson *et al.*[22]	Open	Centre of the cavity	60, 75, 85, 100, 125	0.05, 0.075, 0.1, 0.15	0.05, 0.1, 0.15
Ingason [23]–[25]	Open	Centre of the cavity	32, 42, 59, 75	0.05, 0.075, 0.1	0.05, 0.075, 0.1
Livkiss *et al.* [20]	Open	Near the wall	16.5, 24.8, 32.3, 40.4	0.02, 0.03, 0.04, 0.05, 0.06, 0.1, one wall	N/A
Current study	Open Closed	Entire cavity	20, 35, 50, 74	0.05, 0.1, 0.15	N/A

The majority of these studies were not conducted with modern façade configurations in mind, since burners with a fixed nozzle width were used, whereas in a real fire the flame may be expected to fill the cavity or otherwise be proportional to the cavity width. Even if the behaviour of the flame height was shown to follow similar trends as a function of the cavity width and heat release rate, the models proposed for the flame height have not yet been reconciled between the studies. This indicates the presence of extra variables that might influence the underlying fire dynamics. A comparison of the flame height data against the correlation developed by Ingason for flame height as a function of the heat release rate per unit area (Eq. 8) is presented in Figure 3. The equation proposed by Ingason cannot accurately predict the flame length for the different setups. Hence, a further exploration of the variables of the system is necessary to find the correlations that describe the fire dynamics for full-width burning cavities, as relevant to façades today.

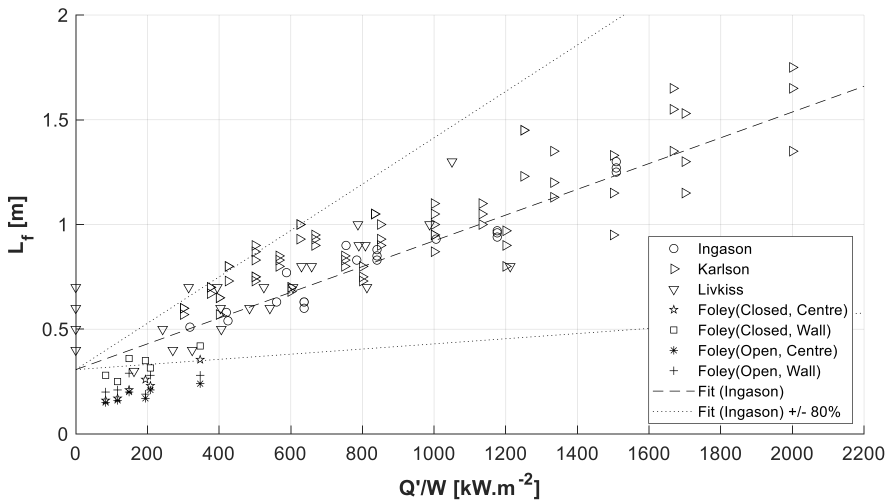

Figure 3. Experimental flame heights vs heat release rate per unit area from Livkiss *et al.*, Karlsson *et al.,* Ingason and Foley [19], [20], [22], [23]. The correlation proposed by Ingason is presented as a dashed line.

Torero argued that cavity width has an important effect on the rate of flame spread. An extremely large cavity will diminish radiative exchange and buoyancy-driven chimney effects, which will generate a flame spread rate similar to the ones observed for a fire against an individual open wall, i.e., when no cavity is present. Contrarily, an extremely narrow cavity will present a blockage of the gas flow caused by the thermal expansion of the combustion gases. This will ultimately cause the flame to cease to spread inside the cavity [27]. Some research has been performed on cavities featuring combustible linings to determine the effect of the cavity on the upward flame spread over the materials [28]–[31]. An extensive series of work has been performed at FM Global using parallel plates setups to simulate the same radiative view factor as in the corner configuration, ensuring an equivalent heat exposure [31]–[33]. This in order to create a sufficiently strong exposure to evaluate full facade systems and predict behaviour in the large-scale corner tests [32]. The work by Nam *et al.* provided an intermediate-scale testing methodology as a screening tool to assess wall and ceiling assemblies for material flammability. This research intended to deliver a testing methodology that allowed to predict full scale test behaviour by using material properties determined at bench scale. Additional studies have been performed to characterise the fire dynamics of ventilated façades featuring combustible elements [34]–[36]. Garvey *et al.* proposed a methodology to isolate the effect of the individual materials on the upward flame spread [34]. However, it was not possible to explore the effect of the cavity width in any of these studies, since a fixed value was used for this parameter.

3. Methodology

The experimental setup consisted of two 600 mm wide, 1800 mm high, 25 mm thick, vermiculite walls (Skamol V-1100 (375), see Table 2 for thermal properties), placed in parallel configuration separated by an air gap, and mounted on an aluminium frame (see Figure 4. a) and b). The dimensions of the non-combustible walls were set considering the dimension of experimental setups used in previous studies [19], [20], [22], [23] and considering the standard size available for construction materials.

One of the walls (denoted as Auxiliary wall in figure 2 a)) was mounted on movable elements that allowed simple and rapid modification of the cavity air width for different experiments. The non-combustible walls were replaced between the experiments after signs of deterioration were detected e.g. cracks.

A sand methane burner was placed at the base of the parallel walls to generate fires with different heat release rates per unit length. The heat released was controlled by using a Teledyne HFC-D-303B mass flow controller. The sand was used to guarantee a uniform distribution of the fuel flow and a uniform heat release rate per unit length of the burner. The width of the burner was modified by partially covering the upper surface with a non-combustible material to obtain the desired width to match the set cavity width. A rectangular burner with a modifiable width meant that it was possible to have the flame present through the entire width of the cavity, instead of being limited to a single fixed nozzle width for all tests, as in previous studies [19], [20], [22], [23]. This ensured that the flame impinged both cavity walls instead of a single lining thereby creating a more onerous scenario [17]. This burner configuration ensures that the test conditions are representative of a realistic scenario for a fire in ventilated façade compared to previous research.

The width of the cavity was also modified as one of the parameters of the tests. The length of the burner was kept constant at 480 mm. It was set to be shorter than the wall width (600 mm) to ensure that flames would not escape the cavity. The combinations of cavity width and HRR were set so the flames did not extend above the top of the walls or outside from the edges of the walls.

Table 2. Temperature dependant thermo-physical properties of the non-combustible boards and TSC materials

Material	Thermal conductivity [W.m^{-1}.K^{-1}]	Density [kg.m^{-3}]	Specific heat capacity [J.kg^{-1}.K^{-1}]	Emissivity [-]
Vermiculite (SKAMOL V-1100(375) [37])	0.12 @ 200°C 0.15 @ 400°C 0.16 @ 600°C	375 @ 20°C	0.94	Not used

	0.19 @ 800°C			
Inconel	15 @ 200°C 18 @ 400°C	7800 @ 20 < T < 1000 °C (T in °C)	$450 + 0.28T - 2.91 \cdot 10^{-4}T^2 + 1.34 \cdot 10^{-7} \cdot T^3$ @ 20 < T < 1000 °C (T in °C)	0.44 to 0.36 @ 216 < T < 490°C

Two arrangements were introduced to study the effect of the air entrainment on the behaviour of the fire (see Figure 4. c). In one of them, the vermiculite boards were located in contact with the burner to prevent air entrainment at the base, this configuration will be called “closed base”. In another configuration , the experimental rig was lifted up 80 mm from the position in the closed base configuration in order to allow the air entrainment from the bottom of the walls, this configuration is denoted “open base”. As the opening size was not varied the influence of this parameter – beyond the presence or absence of an 80 mm opening - on the fire dynamics cannot be determined from the results of these tests . The experimental configurations which were investigated are presented in Table 3.

For each cavity width, three burner heat release rates were tested sequentially one after another within the same experiment. This was to increase the number of tests that could be performed rather than waiting for the apparatus to cool between each test which would be highly time-consuming. For each heat release rate, the test was run until a quasi-steady state was achieved as measured by the TSCs, which took a minimum of 10 minutes and up to 15 minutes. The data was then extracted from a 90 s window within those steady state conditions, and those are the results presented in this manuscript. Every test was carried out twice in order to demonstrate the repeatability of the flame height and external heat flux when following the same experimental procedure.

Table 3. Experimental campaign conditions.

Test	**Cavity width (W) [mm]**	**Q'(Nominal) [kW.m^{-1}]**	**$\dot{Q}'$ (Real) [kW.m^{-1}]**	**Base configuration**
C1	50	20, 35, 50	20.8,36.4,51.56	Closed
C2	50	20, 35, 50	20.8,36.4,52.03	Closed
C3	100	20, 35, 50	20.8,36.4,52.03	Closed
C4	100	20, 35, 50	20.8,36.4,52.06	Closed
C5	150	35, 50, 74	36.41,52.06,79.73	Closed
C6	150	35, 50, 74	36.46,52.06,77.37	Closed
O1	50	20, 35, 50	20.8,36.5,52.06	Open
O2	50	20, 35, 50	20.8,36.6,52.03	Open
O3	100	20, 35, 50	20.8,36.6,52.12	Open
O4	100	20, 35, 50	20.8,36.5,52.08	Open
O5	150	35, 50, 74	36.44,52.05,77.25	Open
O6	150	35, 50, 74	36.44,52.05,78.32	Open

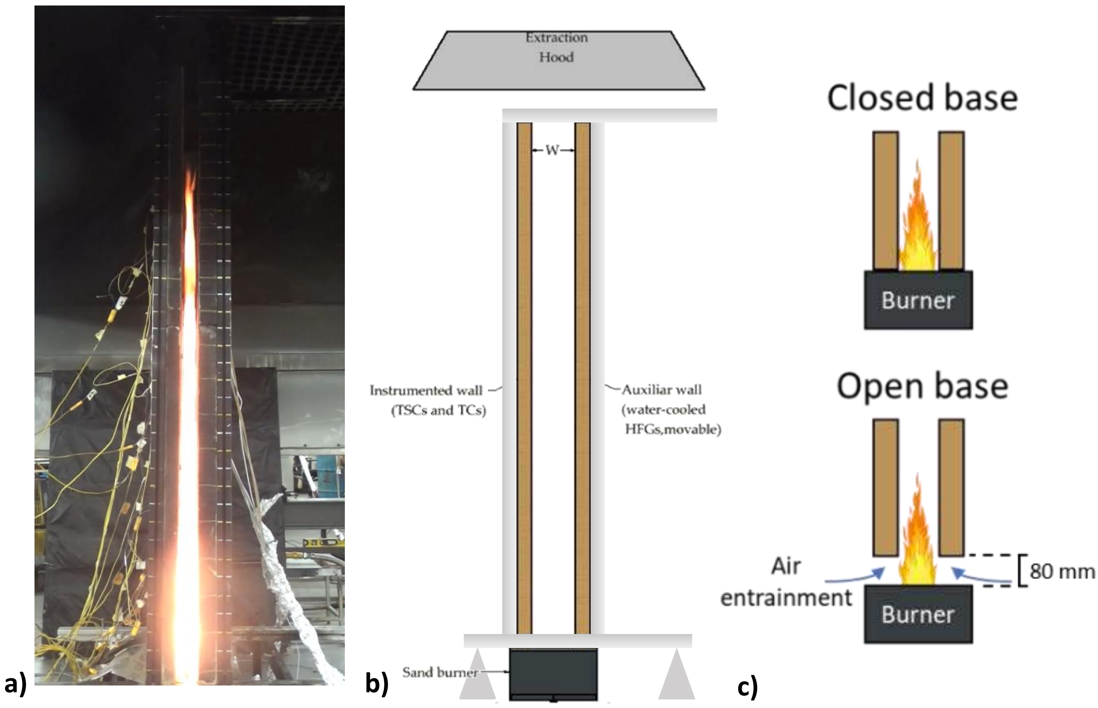

Figure 4. a) Image of the experimental setup. B) Schematic representation of the main components of the experimental setups. c) Base configurations for air entrainment. The blue arrows represent air entrainment at the base of the walls.

The burner heat release rate was calculated as the product of the mass flow rate of the natural gas and its effective heat of combustion (approximately $52.5 \cdot 10^3$ $\mathrm{kJ \cdot kg^{-1}}$). Additionally, the testing rig was placed under an extraction hood in order to verify the heat release rate of the burner using the species evolution approach (both Oxygen consumption [38] and Carbon Dioxide Generation calorimetry [39]). All the tests were recorded with a video camera, located at a height of 1.3 m and a distance of 2 m from the setup (see Figure 5. e), in order to extract the visual flame height of the fire generated by the burner.

3.1. Flame height determination

Flame heights were measured as the tip of the continuous flame from 2250 photos corresponding to all the frames of the 90 s span. A height reference was incorporated in the walls of the setup in order to calibrate the height of the camera. The flame height was initially calculated as the average of the measurements and then corrected to account for the view angle for the camera. To do so, the location of the flame tip was assumed to be in the middle of the burner total length. This is supported by observations made during the experimental campaign and from the external heat flux distribution on the walls (see Section 5). In order to verify the reliability of the flame height data, a repeatability test was performed to measure the relative deviation of the flame height for the sets of experiments (i.e. a test and its repetition).

3.2. Heat flux measurement

One of the walls was instrumented with 15 thin skin calorimeters (TSCs) to measure solid phase temperature used in the calculation of the incident radiant heat flux. These were made of 10 mm diameter, 1.3 mm thickness Inconel discs mounted on 50 mm diameter vermiculite cores inserted in the wall. Additionally, 15 gas-phase thermocouples (TCs, 1.5 mm diameter, type K mineral-insulated metal-sheathed (MIMS)) were installed in this wall to measure the gas-phase temperature at vicinity of the solid surface. These measurements were used in conjunction with the temperature of the TSCs to calculate the radiative incident heat flux on the instrumented wall ($\dot{q}_r''$). The position of the instrumentation is depicted in Figure 5. The opposite wall was instrumented with two Hukseflux water cooled heat flux sensors at heights of 0.65 m and 1.3 m above the edge of the wall. The measurements from the heat flux gauges were compared against the trends for the calculated total external heat fluxes, obtained from the TSC and TC measurements (see Heat flux calculation). This comparison is made to validate the precision of the TSC results and to be able to compare the magnitude of the total external heat fluxes in the wall with those obtained by Foley [19], who used water-cooled heat flux gauges for the measurements. The heat flux measurements reported correspond to the average of 90 measurements in a steady state, corresponding to the same time span when the flame heights were determined.

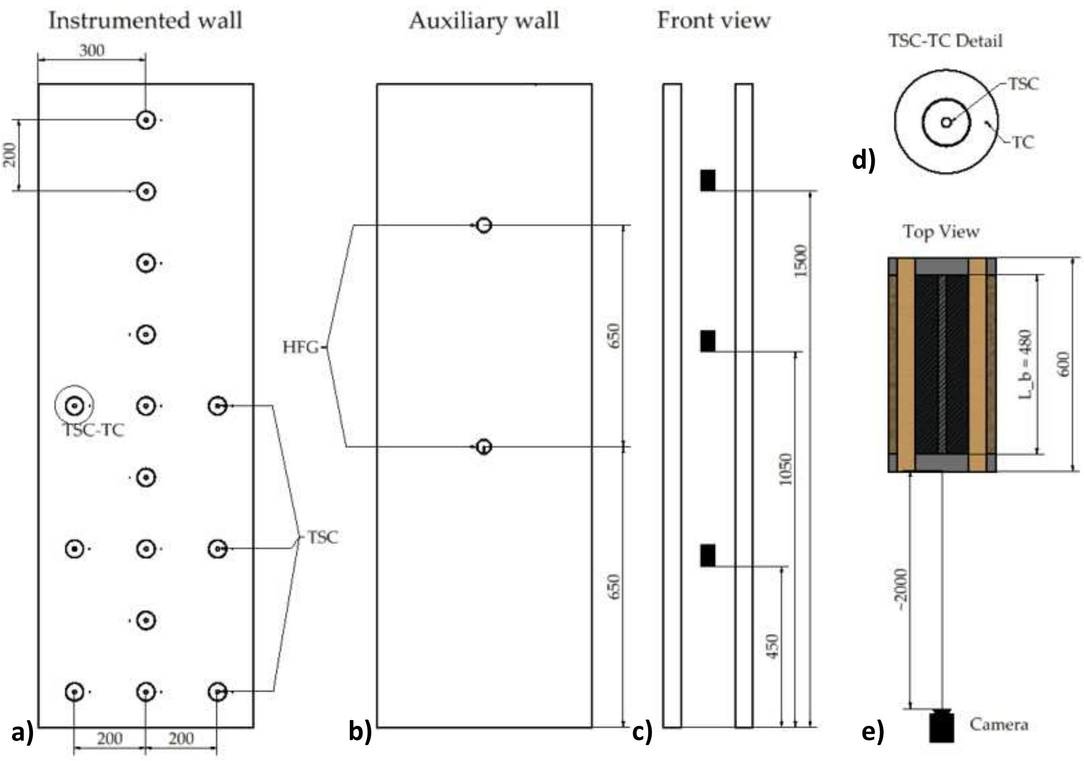

Figure 5. a) Location of the Thin skin calorimeters and gas phase thermocouples in the instrumented wall. **b)** Heat flux gauges in the Auxiliary wall **c)** Front view and location of the velocity probes. **d)** Detailed position of the gas phase thermocouples. **e)** Camera positioning from top view.

3.3. Heat flux calculation

Heat transfer from flames is mainly attained by radiation and convection. The relative significance of these heat transfer mechanisms under different scenarios is of interest, both to increase understanding of heat transfer from flames to the linings of a cavity and to suggest appropriate fire protection measures. The total external heat flux ($\dot{q}''_T$) on the wall was defined as the sum of a radiative and a convective component:

$$\dot{q}''_T = \dot{q}''_r + \dot{q}''_c \tag{11}$$

The convective component was defined as:

$$\dot{q}''_c = h_c\left(T_s - T_{gas}\right) \tag{12}$$

where T_{gas} is the temperature of the gas in the cavity measured with the gas-phase thermocouples, T_s is the solid temperature measured by the TSC), and h_c is the convective heat transfer coefficient. The convective heat transfer coefficient (h_c) was calculated using Eq.13.

$$h_c = k_g \left(\frac{\mathrm{Nu}}{L_c}\right) \quad (13)$$

where k_g is the gas conductivity and L_c is the characteristic length. The Nusselt number was calculated using two different approximations. One for the natural convection regime ($\mathrm{Nu_{NC}}$, see Eq. 14) [40], [41] and for the forced convection regime ($\mathrm{Nu_{FC}}$, see Eq. 15) [42].

$$\mathrm{Nu}_{NC} = 0.68 + \frac{0.67\mathrm{Ra}^{\frac{1}{4}}}{\left(1 + \left(\frac{0.492}{\mathrm{Pr}}\right)^{\frac{9}{16}}\right)^{\frac{4}{9}}} \quad (14)$$

$$\mathrm{Nu}_{FC} = 0.037\mathrm{Re}^{\frac{4}{5}}\mathrm{Pr}^{\frac{1}{3}} \quad (15)$$

Where the Reynolds number (Re) was calculated from the velocities obtained using bidirectional velocity probes with a 0.015 m diameter. The three velocity probes were located in the centreline of the wall and in an equidistant point between the walls. The probes were located 450, 1050 and 1550 mm above the burner (see Figure 5. d).

It was estimated that using either of the approximations would lead to a deviation not higher than 1 $\mathrm{kW.m^{-2}}$ in the convective heat flux component, which is negligible considering the order of magnitude of the incident radiant heat flux (see Eq. 16). Hence, the natural convection approximation was used, since it provided a greater number of locations for the characterisation of the convective and total convective heat flux [43].

The radiative heat transfer flux to the wall was then calculated using the methodology proposed by Hidalgo *et al* [44], as described by Eq.16:

$$\dot{q}_r'' = \frac{1}{\alpha_{TSC} \cdot (1 - C)}\left[\rho_{TSC} \cdot \delta_{TSC} \cdot C_{P_{TSC}} \cdot \frac{dT_s}{dt} + \varepsilon_{TSC} \cdot \sigma \cdot T_s^4 + h_c \cdot (T_s - T_{gas})\right] \quad (16)$$

where α_{TSC} is the absorptivity of the TSC metal disc, C is a correction factor for the heat transfer by conduction, ρ_{TSC} is the density of the TSC metal disc, δ_{TSC} is the thickness of the disc, $C_{P_{TSC}}$ is the specific heat capacity of the disc, ε_{TSC} is the emissivity of the disc, σ is the Stefan-Boltzmann constant, T_s is the solid-phase temperature measured by the TSC.

For the measurement of the incident radiant heat flux in a semi-steady state it can be assumed that the term for the variation of the temperature of the solid can be approximated to 0 (see Eq. 18) and the energy stored by the metal disc can be neglected.

$$\frac{dT_s}{dt} \approx 0 \quad (17)$$

4. Flame height

The results of the average flame tip heights are shown in Figure 6 as a function of the cavity width. These parameters are both normalised by the heat release rate as part of a dimensional analysis for rectangular gas burners based on the work developed by Thomas *et al.* [45] and later used by Quintiere *et al.* [46]. This takes the dimensionless Froude number as the base to compare burners with different sizes and heat release rates. It is clear that for both open and closed based configurations, the flame height dramatically increases with narrower cavity widths and large HRRs. This aligns with previous findings by Karlsson *et al.* [22], who generated a power law model (see Eq. 7) and hinted to the existence of two different regimes, one where the flame height is drastically influenced by the cavity width and heat release rate per unit length burner and one where the influence is less significant. Two different regions were defined for this study considering that the flame height drastically increases when $W/Q'^{2/3} < 0.008$ (narrower cavity widths and large HRRs), whereas the effect is less evident pronounced for the rest of the cases. A piecewise function was therefore proposed to predict the normalised flame height (Eq. 18 and Eq. 19).

$$L_f/Q'^{\frac{2}{3}} = 8.0 \cdot 10^{-4} \left(W/Q'^{\frac{2}{3}}\right)^{-0.878}; \qquad W/Q'^{\frac{2}{3}} < 0.008 \tag{18}$$

$$L_f/Q'^{\frac{2}{3}} = -0.68\,(W/Q'^{\frac{2}{3}}) + 5.96 \cdot 10^{-2}; \qquad W/Q'^{\frac{2}{3}} > 0.008 \tag{19}$$

A significant difference is observed between the open and closed base configurations when the narrowest cavity and the two highest heat release rates were combined ($W/Q'^{\frac{2}{3}} < 0.006$). In those cases, the open base configuration led to higher flames. This might indicate that air entrainment from the base helps push the flame towards the centre of the cavity, away from the walls. The influence of air entrainment on the elongation of the flame does not seem to be significant for the rest of the configurations. The results of the current study are compared with previous studies developed by Livkiss *et al.*[20], Ingason [23] and Karlsson *et al.* [22]. The nondimensional flame heights for the study by Foley and Drysdale are not included since the intention of that research was not to characterise the flame height but the heat transfer [18], [19]. In all cases, the general trend is for flame length elongation as either the cavity width is reduced or as the burner heat release rate is increased. This effect is most pronounced at small cavity widths, and a seemingly asymptotical value is reached as the setup tends to open burning at very large cavity widths. This similarity indicates that the behaviour of the cavity flame is controlled by similar physical phenomena in spite of the experimental setup differences.

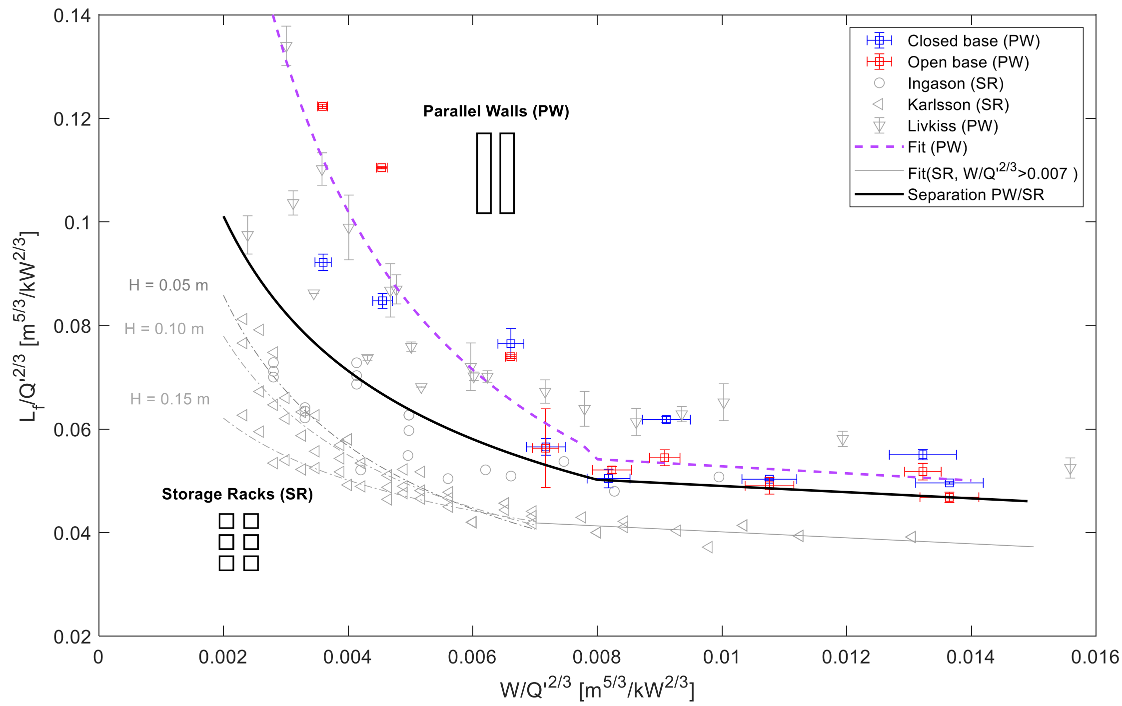

Figure 6. Average normalised flame heights ($L/Q'^{2/3}$) from this study and the studies by Livkiss *et al.*, Karlsson *et al.*, and Ingason [20], [22], [23]. Error bars correspond to the minimum and maximum point from the repetitions for each experiment.

The trend in all the data is similar, and the current study follows the data from Livkiss *et al.*, which had the most similar setup focused on a wall cavity scenario (above the black line in Figure 6). Conversely, although the data for the other two studies (Ingason and Karlsson, both focused on rack storage systems scenario, below the black line in Figure 6) follow a similar trend and the overall flame heights are significantly lower. Specifically, the current study shows approximately 52% higher flames for the open base configuration compared to Karlsson *et al.*, 24.5% higher compared to Ingason, and 2.2% lower compared to Livkiss *et al.* A shorter flame length is expected for the studies by Ingason and Karlsson due to the presence of gaps in the vertical direction in the rack storage setups – as described in the Introduction section – which enabled the air entrainment in several heights of the gap. The results presented here therefore appear to confirm that flame heights are consistently different between rack storage system (with additional vertical cavities) and ordinary cavity flame heights where the two walls are parallel with no vertical cavities. The presence of these cavities in the vertical direction has a considerable effect and decreases the flame height significantly. This is expected to be because these cavities enhance the cold air entrainment, which cools down the plume, generating a decrease on the buoyancy and leading to a shorter plume. Additionally, the higher availability of air at lower heights due to the vertical cavities implies that the combustible gas can be mixed with the oxidiser at lower heights and is consumed at a lower height from the burner. Last, the geometry of the storage rack, especially the sharp edges might enhance flow shearing, promote the air-combustible mixing which allows the reaction to occur at lower heights, leading to shorter flames if compared to the parallel wall setup.

There are still some differences in the cavity flame heights presented here and those of Livkiss *et al.*, particularly at large cavity widths. This is likely because of the difference in the type of burner used in both studies. A flame produced by a sand burner (in this study) should be affected less by the momentum of the gases from the burner compared to a flame produced by a line burner (in Livkiss' study). Additionally, having the burner next to the wall would generate taller flames compared to the burner used in this study, which filled the whole cavity, due to the difference in the aspect ratio of the burners. Further discrepancies could be attributed to the variation within the techniques for the measurement of the flame, since Livkiss and the current study used different frequency for the flame height acquisition and different treatment for the effect of the view angle of the camera.

From all the above, it is clear that the flame height is highly sensitive to changes in the geometry of the system, the heat release rate of the fire source, and the restriction of the air supply. The results here suggest that parallel plates setups with no vertical gaps have consistently larger flame heights compared to storage rack systems. The exact impact of the vertical gaps has not been quantified here given that this is not particularly relevant for façade scenarios, since the inclusion of these additional gaps leads to the entrainment of cold air and to a lower heat exposure of the walls, thereby representing a less onerous scenario. Furthermore, air entrainment through vertical gaps appears to influence the system but has not been included in the current scope. To explore some of the differences in the results further, the total external heat flux helps describe some of the dynamics within the cavity.

5. Total external heat flux

The total external heat flux (refer to Eq. 11) as a function of height is presented in Figure 7. As with the flame heights, there are clear distinctions for different burner HRR, with higher HRR consistently giving higher total external heat flux across the height of the wall. The data from TSCs and heat flux gauges is plotted to enable a comparison of the results from the two instruments. It can be seen that the calculations for the centreline total heat flux follow a trend and that the values do not deviate significantly from the measurements obtained by the water-cooled heat flux gauges. This is because the thin skin calorimeters are calibrated using the heat flux gauges and both the calculation and measurement are linked by using the correction factor (C) in Eq. 16 . This allowed a comparison of these results with external heat flux measurements performed by Foley & Drysdale [19]. A comparison of closed base (left) and open base (right) also shows that a higher external heat flux is registered in the wall for the closed base scenario compared to the open scenario condition, and the highest external heat flux is close to the burner as would be expected.

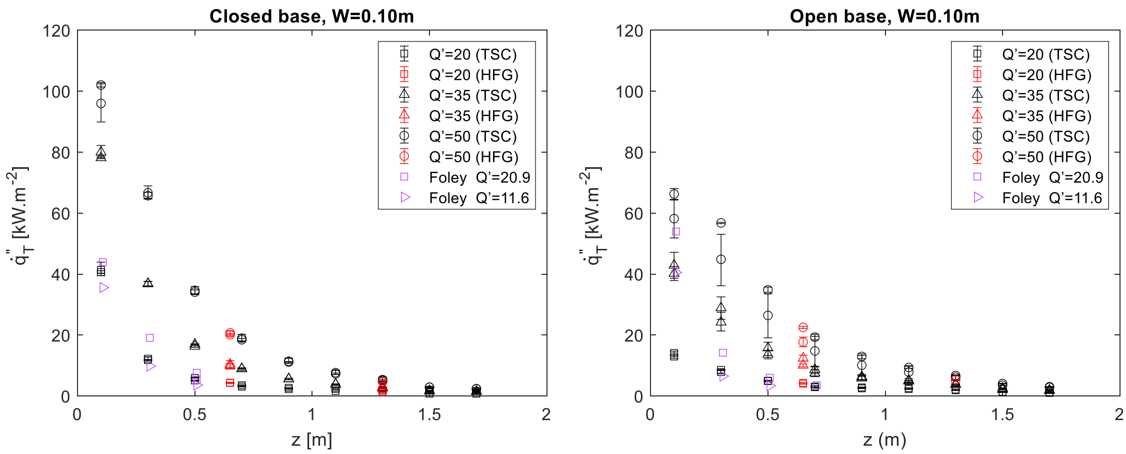

Figure 7. Centreline total external heat flux measured by heat flux gauges(HFG) and calculated from TSCs. Error bars correspond to the 20^{th} and 80^{th} percentile of the measurements for the steady state span.

The difference observed between the closed and open scenarios is because the flame fills the whole cavity and impinges both walls in the case of the closed base. When the base is open, cool air flows upwards from the base and comes between the flame and the walls, preventing direct flame impingement and reducing the total external heat flux. Flame impingement increases the temperature of both walls and generates a larger radiative exchange between the two surfaces.

The cavity width also had influence on the heat transferred to the walls of the cavity. The increase of the cavity diminishes the view factor between the two surfaces. The effect on the view factor was quantified using Eq. 6 and the spatial variation for the view factor along the plate for the three different cavity widths was calculated and is presented in Figure 8. This change in the view factor ultimately leads to an enhancement of the thermal exchange between the surfaces.

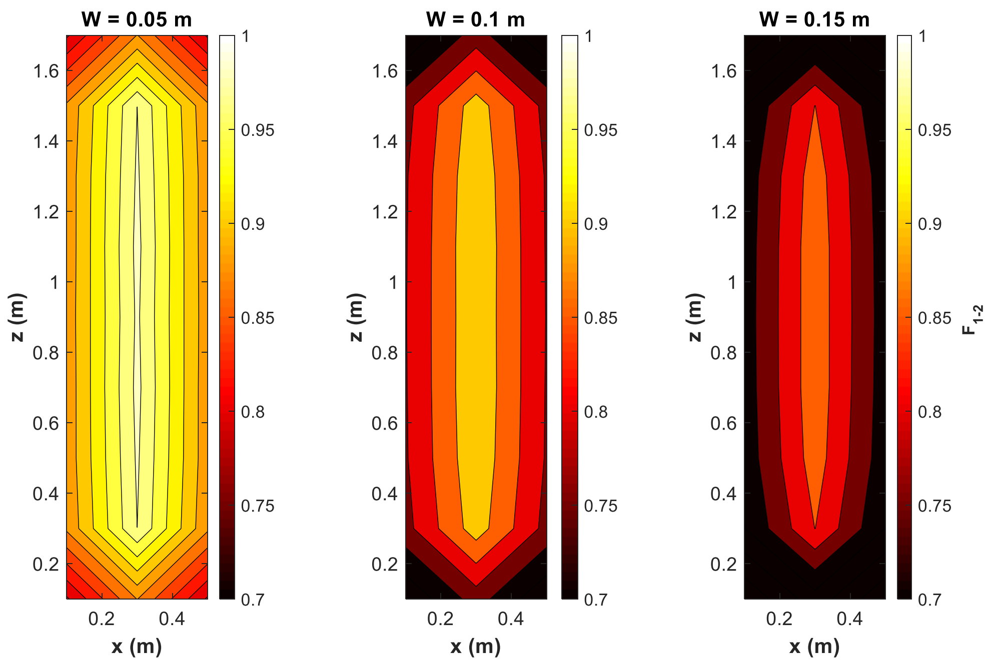

Figure 8. Spatial variation of the view factor between the two parallel walls.

It was determined that for the widest cavity, each wall is receiving only 80 % as much energy from the opposite wall as it did in the narrowest cavity. Also, a significant drop in the view factor is observed away from the centre points of the walls, due to the geometric configuration of the walls. This implies a lower radiative exchange between the two walls. It is possible to observe that although the flame heights are similar for both base configurations, the behaviour of the total external heat flux is different. A deeper study considering the influence of the air entrained on the heat flux distribution was conducted to explore the mechanisms underlying the discrepancies to explain this behaviour.

5.1. Influence of air entrainment

The TSCs located distant from the centreline of the wall (see Figure 5 (a)) were used to quantify the spatial variation of the total heat flux over the wall. A subset of the results is presented in Figure *9*. It is evident that for both open and closed based configurations, the flame is symmetrically distributed and that the flame tip is present at the middle of the centreline, where the highest heat flux value is present. A decay of the heat flux towards the edges of the wall can be observed. This can be explained by the change in the view factor and by the air entrainment from the open sides of the setup. The view factor at the lateral edges is lower than at the centreline of the wall, which implies a lower radiative heat transfer. As for the air entrainment, this process could only happen laterally, via the cavity when the base was closed. The entrainment decreased as the cavity width was reduced. This causes the flame to be pushed towards the centreline of the walls (x=0.3 m) by the incoming air. This effect would also happen in a similar but wider setup. Conversely, when the base is open, air is entrained both vertically from the bottom of the burner and horizontally through the cavity between the walls. Also, it was observed during the experiments that for the closed base, the flame behaved as a uniform sheet filling the entire cavity, whereas for the open scenario, the flame impinged the walls for a shorter distance. A more detailed understanding of the heat transfer behaviour was sought through the study of the heat transfer mechanisms to determine the influence of the different factors on the external heat flux and propose adequate design measures that diminish the level of exposure from the dominant heat transfer component.

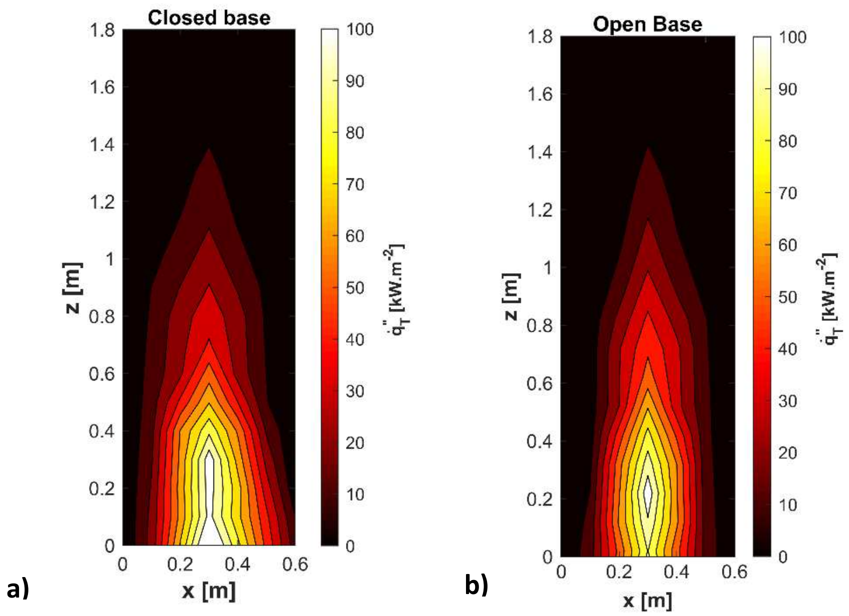

Figure 9. Heat flux spatial distribution a) HRR = 35 kW.m^{-1}, W = 0.05 m, closed base b) HRR = 35 kW.m^{-1}, W = 0.05 m, open base

5.2. Dominant heat transfer mechanism

The magnitude of the radiative component and its dependence on the cavity width and height from the fire source was characterised as the ratio between the radiative heat transfer and the total heat transfer. This ratio is presented for different configurations in Figure 10.

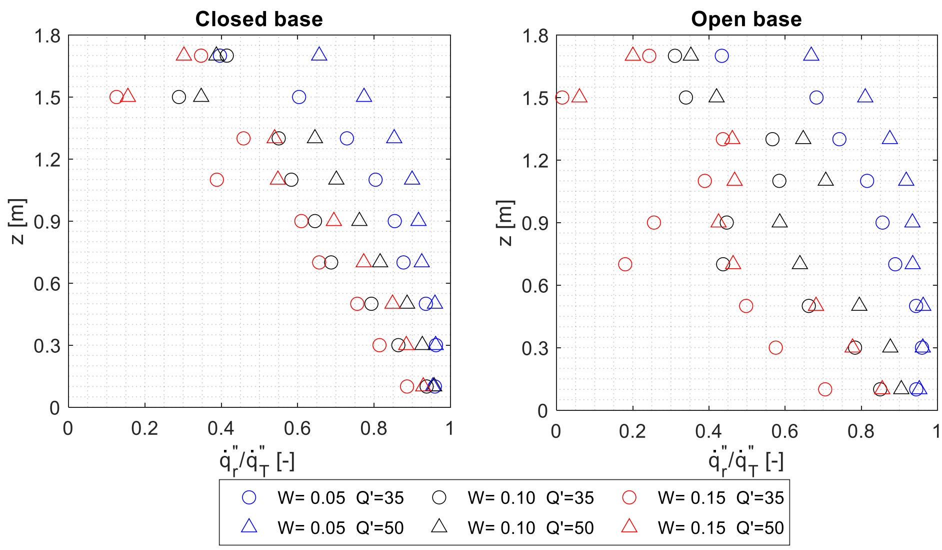

Figure 10. Contribution of the radiative heat flux component to the total external heat flux vs setup height

A decrease of the contribution of the radiative component can be observed as the cavity width increases, due to the reduction of the view factor and hence the radiative exchange between the two surfaces. Additionally, a decrease in the significance of the radiative component can be observed for all the configurations as the height above the burner increases. This could be explained by the absence of the flame at the upper region of the walls. The significance of the radiative component follows a similar trend for both the open and closed configurations. However, it can be noticed that this ratio decreases more significantly in the open base configuration. The increase in radiation in the closed base scenario arose from restricting air access for combustion, causing a thickening of the flames. This phenomenon can also explain the increase in the radiative component when the cavity width is reduced. It was also expected for radiative exchange between the walls to decrease with increased separation. The generalisation of this behaviour would require experiments in a wider range of conditions. However, the results obtained highlight the importance of radiative heat transfer between surfaces that restrict a fire. A system where heat transfer is dominated by radiative heat transfer is more easily scalable, since the effect of the heat losses by convection can be neglected.

5.3. Dimensionless correlations for the external heat flux as a function of the system variables

Correlations were sought for the calculated total external heat fluxes and their dependence on the system variables (i.e. cavity width, heat release rate per unit length of burner, aspect ratio of the burner, height from the base of the burner). First, the dependence on the spatial variation and the dimensionless height, $z/(Q'^{*\frac{2}{3}} \cdot L_b)$, based on previous work by Hasemi [26] and Thomas *et al.* [45], was studied. A subset of the data consisting of the cases with the same heat release rates per unit length burner and data from Foley and Drysdale [19] are presented in Figure 11.

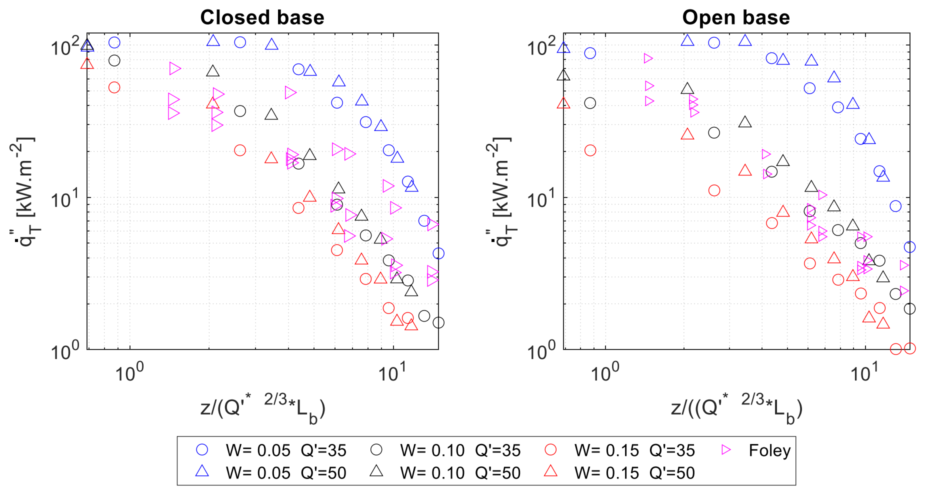

Figure 11. Heat flux as a function of the dimensionless height

Figure 11 shows the influence of the cavity width and the heat release rate on the total external heat flux. For both open and closed base configurations, the cavity walls are exposed to a greater external heat flux as the cavity width is decreased. Also, it is possible to observe that a higher heat release rate of the burner led to higher heat fluxes, as expected. A considerable dispersion between the data series corresponding to different cavity widths was observed, which indicated the inclusion of an extra parameter accounting for the geometry of the burner was necessary to model the behaviour of the total external heat flux.

A term considering the aspect ratio between the cavity width and the burner length was then included to explore the effect of changing this variable. The exponent for the aspect ratio was set to 0.9 after an optimization process that aimed to minimise the dispersion of the data in the plume region. Data obtained by Foley [18] for the same dimensional groups were adjusted to the format of the obtained correlations (Eq. 20) and are presented along the experimental data for this study in Figure 12. The delineation between the flame and the plume that is shown in Figure 12 is based on the variation of the incident heat flux on the wall, which is minimal in the flaming region as opposed to in the plume region where a sharp decay of the incident heat flux to the wall can be observed. This approach is consistent with the work by Back [16].

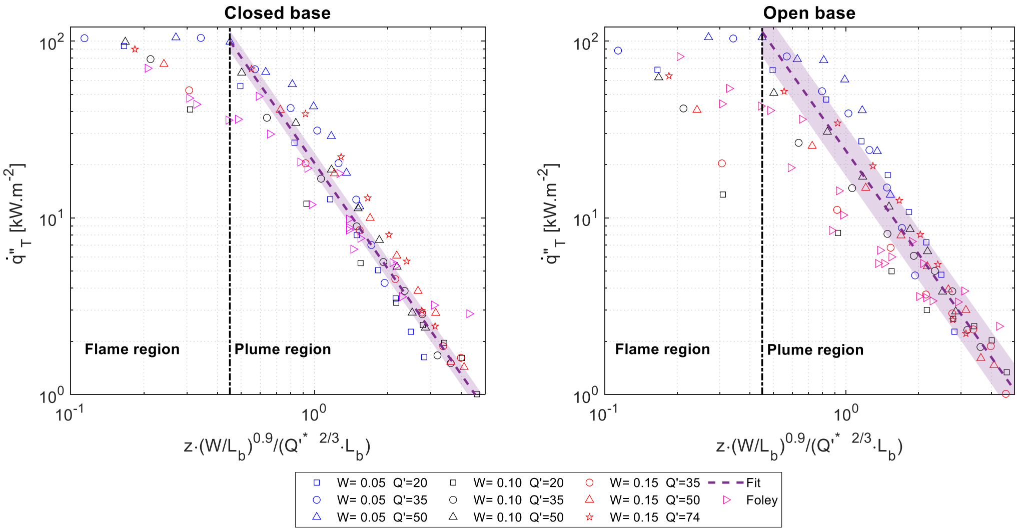

Figure 12. Heat flux as a function of the dimensionless height. The shaded areas represent the 95% confidence bounds

The correlations were limited for the region of the abscissa, where a sudden decrease of the value for the external heat flux was noticed. The correlations obtained are more conservative than the ones obtained by Foley since, in both open and closed scenarios, the value for the prediction of the model is higher than the data obtained in that study. This can be in part attributed to the use of a lower heat release rate for one of the configurations used by Foley. A greater scatter can be observed for the open base configuration. This could imply that the variables used for the correlation might not be enough to predict the behaviour of the total external heat flux, and further studies with different air entrainment conditions should be conducted to obtain a more accurate model.

A set of correlations following the structure presented in Eq. 20 was obtained for the ranges corresponding to the plume region.

$$\dot{q}''_T = C_1 \cdot \left(z \cdot \left(\frac{W}{L_b}\right)^{0.9} / (Q'^{*\frac{2}{3}} \cdot L_b)\right)^{C_2}, \qquad \left[z \cdot \left(\frac{W}{L_b}\right)^{0.9} / (Q'^{*\frac{2}{3}} \cdot L_b)\right] > 0.45 \qquad (20)$$

where C_1 is the model preexponential factor and C_2 is the dimensionless heat flux decay exponent.

A single expression containing the data for both base configurations could be proposed, however the correlation with the combined experimental data is significantly weaker than when the two configurations were treated separately. The coefficients for the two cases contained in Eq. 20, their error margins for the 95% confidence bounds and their respective correlation coefficient are presented in table 4.

Table 4. Error margins corresponding to 95% confidence bounds for the coefficients used in the external heat flux correlations and correlation coefficients.

	Preexponential factor (C_1)	*Exponent* (C_2)	*Correlation coefficient* (R^2)
Closed	20.42 ± 0.96	-1.99 ± 0.11	0.95
Open	23.76 ± 2.4	-1.94 ± 0.37	0.87

It is possible to tell although the correlations present the same structure, the coefficients are different for both open and closed base configurations. A greater scatter is observed for the open base scenario which can be observed in larger error margins for the coefficients. The total external heat flux depends on $\left(\frac{W}{L_b}\right)^{-1.76}$ for the open base scenario, whereas it depends on $\left(\frac{W}{L_b}\right)^{-1.79}$ for the closed base scenario. This means a greater influence of the cavity width for the later configuration. This could be attributed to the additional availability of air at the bottom of the flame and its subsequent effect on the cooling of the walls and the prevention of flame impingement, both leading to a sharper decay on the external heat flux measured at the surface.

It was not possible to determine the underlying causes for the degree of variability of the coefficients for the open and closed base scenarios. This is because in this study only two levels of air entrainment were included and this variable was not quantitatively characterised. The use of CFD tools as well as a detailed quantification of the magnitude of the air entrained in all the directions of the plume might be beneficial to explore the underlying physics in more detail.

6. Conclusions

This paper has investigated the differences in flame heights and heat flux for various cavity fire setups by different authors, and has generated new data for further comparison with these existing datasets. The differences in the behaviour of the flame between the different configurations has been explained by an analysis of the underlying mechanisms that govern the fire and its interaction with the surroundings.

The obtained data for the normalised flame heights follows a similar trend to previous studies, which point to similar governing mechanisms for the fire dynamics in cavities. The differences among setups can be mainly attributed to the presence of additional vertical gaps in rack storage systems that cause a decrease in the elongation of the flame. Other sources of variability can be the position of the flame in the cavity and the type of burner as well as the use of different methods to record the flame height.

An increase of the total external heat flux on the walls was observed when the separation between the walls was decreased because of different reasons. First, the heat exchanged among the surface comprising the cavity increases because a relative increase of the view factor. Besides the cavity size, air entrainment at the bottom of the walls was shown to have an influence on the external heat flux. The flow of air from the base reduces the flame impingement on the walls reducing the energy transferred from the flame to the wall. This phenomenon is more significant in the configurations with the 0.10 m and 0.15 m separation. The findings of this research in regards to the influence of cavity width and air entrainment on the external flux received by the walls of a cavity have direct relevance to problems of ignition and upward flame spread in confined spaces which have inward-facing combustible surfaces, such as ventilated facades.

It was found that radiation generally dominates the heat transfer, especially near the bottom of the system. A decrease in both convective and radiative heat transfer is noticed when the cavity width is increased. For heights further from the fire source, the heat flux trends indicate that the air entrainment from the sides might be more relevant than the entrainment from the base. However, further studies or measurements on air entrainment would be required to confirm this and obtain more accurate models for both scenarios.

The results of this work are only applicable to the ranges studied, and no consideration has been given to extensive scaling or extrapolation. The conclusions for the "open base" configuration apply to an 80 mm gap at the bottom and the influence of the size of this opening could be the subject of further study. Furthermore, the basic setup is intended to explore the relevant phenomena and their influence on fundamental fire dynamics. The correlations and data obtained for the external heat flux as a function of the cavity width, the heat release rate of the fire and the height of the walls can be used as a design tool if a maximum allowable heat transfer exposure to the combustible linings is set as a test input. Understanding the behaviour in complex façade systems for real buildings requires additional work and careful consideration, since the research presented in this article was executed in a simplified set up with reduced dimensions to focus on the characterisation of the fundamental principles governing the system. Future work could also include further numerical work to verify the applicability of the proposed scaling laws, studying the impact of the addition of a combustible lining in the cavity, varying the aspect ratio between the burner and the cavity, as well as the position of the burner to better understand the implications of these variables in the fire hazard of the system.

Acknowledgements

This project was supported by funding from a University of Queensland EAIT (Engineering, Architecture and Information Technology) Early Career Research Philanthropic grant (No. 2018002400), which is gratefully acknowledged. The authors also wish to thank the technical assistance of Brendan Garvey, Stewart Mathews and Jeronimo Carrascal, and are grateful to Tomas Bravo, Waseem Hittini and Vinny Gupta for helpful discussions.

Nomenclature

C	Thin skin calorimeter correction factor $(-)$
C_1	model preexponential factor$(\mathrm{kW.m^{-2}})$
C_2	dimensionless heat flux decay exponent$(-)$
C_P	specific heat capacity $(\mathrm{kJ.kg^{-1}.K^{-1}})$
Fr	Froude number $(-)$
g	gravitational constant $(\mathrm{m.s^{-2}})$
h_c	convective heat transfer coefficient $(\mathrm{kJ.kg^{-1}.K^{-1}})$
H	vertical cavity size (m)
k_g	gas conductivity $(\mathrm{kW.m^{-1}.K^{-1}})$
K_1	model constant $(\mathrm{kW.m^{-2}})$
K_2	dimensionless burner aspect ratio constant $(-)$
K_3	dimensionless heat flux decay constant $(-)$
L_b	burner length (m)
L_c	characteristic length (m)
L_f	flame height (m)
Nu	Nusselt number $(-)$
Pr	Prandtl number $(-)$
Q	heat release rate (kW)
Q'	heat release rate per unit length of burner$(\mathrm{kW.m^{-1}})$
Q'^*	dimensionless heat release rate $(-)$
$\dot{q}''_c$	convective heat flux $(\mathrm{kW.m^{-2}})$
$\dot{q}''_r$	incident radiative heat flux $(\mathrm{kW.m^{-2}})$
$\dot{q}''_T$	total external heat flux $(\mathrm{kW.m^{-2}})$
R	shortest distance between two surfaces (m)
Ra	Rayleigh number $(-)$
Re	Reynolds number $(-)$
T_{gas}	gas phase temperature (K)
T_s	solid phase temperature (K)
W	cavity width (m)
W_b	burner width (m)
z	height (m)

α_{TSC}	absorptivity $(-)$
δ	thickness (m)
ε_{TSC}	emissivity $(-)$
ρ	density $(\mathrm{kg.\,m^{-3}})$
ρ_{∞}	ambient density $(\mathrm{kg.\,m^{-3}})$
σ	Stefan-Boltzmann constant $(\mathrm{kW.\,m^{-2}.\,K^{-4}})$
θ	surface angle (rad)

References

[1] A. B. Besir and E. Cuce, "Green roofs and facades: A comprehensive review," *Renew. Sustain. Energy Rev.*, vol. 82, pp. 915–939, Feb. 2018.

[2] B. Lane, "The Grenfell Tower Inquiry: Dr Barbara Lane's expert report (supplemental). Phase 1 Report-Section 9 Routes for fire spread out through the window openings," 2018.

[3] B. Lane, "Grenfell Tower Inquiry: Dr Barbara Lane report (Phase 1 - supplemental), BLAS0000001," 2018.

[4] E. Antonatus, "Facades– Fire Safety Aspects in the context of increasing use of Thermal Insulation," in *Interflam 2013: Proceedings of The Thirteenth International Conference*, 2013, pp. 1291–1302.

[5] M. S. McLaggan *et al.*, "Towards a better understanding of fire performance assessment of façade systems: Current situation and a proposed new assessment framework," *Constr. Build. Mater.*, vol. 300, p. 124301, Sep. 2021.

[6] M. S. McLaggan *et al.*, "Flammability trends for a comprehensive array of cladding materials," *Fire Saf. J.*, p. 103133, May 2020.

[7] K. Saito, J. G. Quintiere, and F. A. Williams, "Upward Turbulent Flame Spread.," pp. 75–86, 1986.

[8] J. G. Quintiere and T. G. Cleary, "Heat flux from flames to vertical surfaces," *Fire Technol.*, vol. 30, no. 2, pp. 209–231, May 1994.

[9] B. Karlsson and J. Quintiere, *Enclosure Fire Dynamics*. CRC Press, 1999.

[10] Y. Hasemi and M. Nishihata, "Fuel shape effect on the deterministic properties of turbulent diffusion flames," *Bull. Japan Assoc. Fire Sci. Eng.*, vol. 38, no. 2, pp. 29–34, 1989.

[11] W. Takahashi, O. Sugawa, H. Tanaka, and M. Ohtake, "Flame And Plume Behavior In And Near A Corner Of Walls," *Fire Saf. Sci.*, vol. 5, pp. 261–271, 1997.

[12] O. Sugawa, H. Satoh, and Y. Oka, "Flame Height from Rectangular Fire Sources Considering Mixing Factor," in *Proceedings of the third International Symposium Fire Safety science*, 1991, pp. 435–444.

[13] L. Hu, S. Liu, and X. Zhang, "Flame heights of line-source buoyant turbulent non-premixed jets with air entrainment constraint by two parallel side walls," *Fuel*, vol. 200, pp. 583–589, Jul. 2017.

[14] D. Drysdale, *An introduction to fire dynamics*, Third edit. Wiley, 2011.

[15] Y. Hasemi and T. Tokunaga, "Some Experimental Aspects of Turbulent Diffusion Flames and Buoyant Plumes from Fire Sources Against a Wall and in a Corner of Walls," *Combust. Sci. Technol.*, vol. 40, no. 1–4, pp. 1–18, 1984.

[16] G. Back, C. Beyler, P. Dinenno, and P. Tatem, "Wall Incident Heat Flux Distributions Resulting From An Adjacent Fire," *Fire Saf. Sci.*, vol. 4, pp. 241–252, 1994.

[17] R. B. Williamson, A. Revenaugh, and F. W. Mowrer, "Ignition Sources in Room Fire Tests and Some Implications for Flame Spread Evaluation," in *Proceedings of the third International Symposium Fire Safety science*, pp. 657–666.

[18] M. Foley, "The Use of Small Scale Fire Test Data for the Hazard Assessment of Bulk Materials (PhD thesis)," The University of Edinburgh, 1995.

[19] M. Foley and D. D. Drysdale, "Heat transfer from flames between vertical parallel walls," *Fire Saf. J.*, vol. 24, no. 1, pp. 53–73, 1995.

[20] K. Livkiss, S. Svensson, B. Husted, and P. van Hees, "Flame Heights and Heat Transfer in Façade System Ventilation Cavities," *Fire Technol.*, vol. 54, no. 3, pp. 689–713, 2018.

[21] J. L. De Ris and L. Orloff, "Flame heat transfer between parallel panels," *Fire Saf. Sci.*, pp. 999–1010, 2005.

[22] B. Karlsson, P. H. Thomas, and G. Holmstedt, "Flame Sizes in a Small Scale Stack : Pilot experiments, (LUTVDG/TVBB--3077--SE; Vol. 3077)," pp. 1–10, 1995.

[23] H. Ingason, "Fire experiments in a two dimensional rack storage. Brandforsk Project 701-917.," Boras, Sweden, 1993.

[24] H. Ingason, "Two Dimensional Rack Storage Fires," *Fire Saf. Sci.*, vol. 4, pp. 1209–1220, 1994.

[25] H. Ingason, "Modelling of a Two-Dimensional Rack Storage Fire," *Fire Saf. J.*, vol. 30, no. 1, pp. 47–69, 1998.

[26] Y. Hasemi, “Experimental Wall Flame Heat Transfer Correlations for the Analysis of Upward Wall Flame Spread,” *Fire Sci. Technol.*, vol. 5, no. 1, pp. 121–121, 1985.

[27] J. L. Torero, “Grenfell Tower Inquiry: Professor Jose Torero report (Phase 1 - supplemental), JTOS0000001,” 2018.

[28] M. Coutin, J.-M. Most, M. Delichatsios, and M. Delichatsios, *Flame Heights In Wall Fires: Effects Of Width, Confinement And Pyrolysis Length*, vol. 6. 1999.

[29] S. R. Wasan, P. Van Hees, and B. Merci, “Study of pyrolysis and upward flame spread on charring materials—Part I: Experimental study,” *Fire Mater.*, vol. 35, no. 4, pp. 209–229, Jun. 2011.

[30] H. Y. Wang, J. L. Torero, and P. Joulain, “Calculation of vertical parallel wall fires with buoyancy-induced flow,” *Fire Saf. Sci.*, pp. 671–682, 2000.

[31] R. L. Alpert, “Evaluation of the Hazard of Fire Resistant Materials Using Measurements from Laboratory and Parallel Panel Tests,” pp. 41–57.

[32] S. Nam, J. De Ris, P. Wu, and R. Bill, “From bench-scale test data to predictors of fullscale fire test results,” *Fire Saf. Sci.*, pp. 469–480, 2005.

[33] S. Nam and R. G. Bill, “A new intermediate-scale fire test for evaluating building material flammability,” *J. Fire Prot. Eng.*, vol. 19, no. 3, pp. 157–176, 2009.

[34] B. Garvey *et al.*, “Experimental methodology to study the fire contribution of cladding materials,” in *Interflam*, 2019, vol. 15, no. 2, pp. 2079–2090.

[35] E. Guillaume, T. Fateh, R. Schillinger, R. Chiva, S. Ukleja, and R. Weghorst, “Intermediate-Scale Tests of Ventilated Facades with Aluminium-Composite Claddings,” *J. Phys. Conf. Ser.*, vol. 1107, no. 3, 2018.

[36] G. Agarwal, Y. Wang, and S. Dorofeev, “Fire performance evaluation of cladding wall assemblies using the 16-ft high parallel panel test method of ANSI/FM 4880,” *Fire Mater.*, no. April, pp. 1–15, 2020.

[37] Skamol A/S, “V-1100 (375) Vermiculite insulating boards - Dataheet.” Jul-2012.

[38] M. L. Janssens, “Measuring rate of heat release by oxygen consumption,” *Fire Technol.*, vol. 27, no. 3, pp. 234–249, 1991.

[39] S. Brohez, C. Delvosalle, G. Marlair, and A. Tewarson, “Soot generation in fires: An important parameter for accurate calculation of heat release,” *Fire Saf. Sci.*, pp. 265–276, 2000.

[40] R. B. Bird, W. E. Stewart, and E. N. Lightfoot, *Transport phenomena, second edition*, vol. 1, no. 2. 2012.

[41] F. P. Incropera, D. P. Dewitt, T. L. Bergman, and A. S. Lavine, *Principles of Heat and Mass Transfer*, Seventh Ed. Wiley, 2011.

[42] S. W. Churchill and H. H. S. Chu, “Correlating equations for laminar and turbulent free convection from a vertical plate,” *Int. J. Heat Mass Transf.*, vol. 18, no. 11, 1975.

[43] J. Mendez, D. Lange, J. P. Hidalgo, and M. S. Mclaggan, “Experimental Study of the Fire Dynamics in a Non-combustible Parallel Wall setup,” in *Proc. Tenth Int. Semin. Fire Explos. Hazards*, 2022.

[44] J. P. Hidalgo, C. Maluk, A. Cowlard, C. Abecassis-Empis, M. Krajcovic, and J. L. Torero, “A Thin Skin Calorimeter (TSC) for quantifying irradiation during large-scale fire testing,” *Int. J. Therm. Sci.*, vol. 112, pp. 383–394, 2017.

[45] P. H. Thomas, C. T. Webster, and M. M. Raftery, “Some experiments on buoyant diffusion flames,” *Combust. Flame*, vol. 5, pp. 359–367, 1961.

[46] J. Quintiere, M. Harkleroad, and Y. Hasemi, “Wall Flames and Implications for Upward Flame Spread,” *Combust. Sci. Technol.*, vol. 48, no. 3–4, pp. 191–222, Jul. 1986.